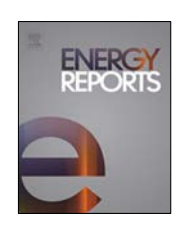


Contents lists available at ScienceDirect

Energy Reports

journal homepage: www.elsevier.com/locate/egyr



Research paper

Potential of petroleum source rock brines as a New Source of Lithium: Insights from basin-scale modeling and local sensitivity analysis



Kyung Jae Lee

Department of Petroleum Engineering, University of Houston, 5000 Gulf Freeway, Building 9, Houston, TX 77204, USA

ARTICLE INFO

Article history: Received 16 October 2021 Received in revised form 19 November 2021 Accepted 29 November 2021 Available online xxxx

Keywords: Lithium Source rock brines Kerogen Basin-scale modeling Fate and transport in subsurface

ABSTRACT

The demand for lithium (Li) has greatly escalated during the past decade and is predicted to increase continuously with the market growth of the electrified transportation and renewable energy, given that Li-ion batteries are the major energy storage method for these sectors. In spite of the urgent need of satisfying the increasing demand of Li, sources of global Li production have been limited in continental brines and pegmatites. In the line with the effort to enhance and diversify the sources of Li supply, this study seeks to predict the production potential of Li from a new source-petroleum source rock brines—and evaluate the most influential factors affecting it. This subject matter is addressed by basin-scale numerical simulation combined with local sensitivity analysis. The numerical simulation with a conceptual model of petroleum source rock system addresses the accumulation of Li in various locations, by taking account for the release of Li from kerogen decomposition reaction in organic-rich source rock, and fate and transport of expelled Li as interacting with reservoir rock. In combination with the numerical simulations, the impacts of various parameters on the Li mass fraction in brines at various observation points are quantified, by conducting local sensitivity analysis. It elucidates the relative sensitivity of Li production potential to the parameters of Li stoichiometry in kerogen decomposition reaction, Na-Li equilibrium coefficient, Na-clay mass fraction in solid phase, Li-clay mass fraction in solid phase, and Na ion mass fraction in brines. Our results provide the conceptual information of most important parameters to be investigated to quantitatively predict the Li production potential from brines at various locations in the petroleum source rock systems that can be used to contribute to the enhancement and diversification of the Li supply.

© 2021 The Author(s). Published by Elsevier Ltd. This is an open access article under the CC BY-NC-ND license (http://creativecommons.org/licenses/by-nc-nd/4.0/).

1. Introduction

Tackling climate change is one of the most critical challenges that global society faces today, and it has raised the need of decarbonizing energy use to reduce the emissions of greenhouse gas. The most significant and efficient ways to achieve the decarbonization of energy use include the electrification of transportation and the increase of renewable energy in electricity generation. As lithium (Li)-ion batteries are the major energy storage used for both electric vehicles and renewable solar-and-wind electricity generation, the demand for Li has greatly escalated during the past decade and is predicted to increase continuously with the market growth of electric vehicles and renewable power generation (Gielen et al., 2019; USGS, 2020). Despite the urgent need of satisfying the increasing demand of Li, sources of global Li production have been limited in continental brines and pegmatites (Schulz et al., 2018; USGS, 2020). To diversify and enhance the sources of global supply of critical minerals including

involve the brines in source rock where kerogen occurs, reservoir

rock where released Li dissolved in water flows through, and formation where transported Li is accumulated (Fig. 1). Despite the promising potential of Li, current state of the science lacks the knowledge and understanding of fundamental phenomena relevant to the origin, fate, and transport of Li in source rock brines, because the two main scientific research areas for petroleum systems and Li geochemical cycle are uncombined. For example, the discipline of petroleum engineering has built a systematic

knowledge in petroleum source rocks by addressing the fate

Li, countries around the world are making various efforts to develop advanced technologies of their exploration and exploitation. In line with the effort to provide the stable supply of Li, this

study seeks to characterize Li accumulated in petroleum source

rock brines through a basin-scale modeling approach, given the

recently found potential of petroleum source rock brines as a

substantial source or Li (Clauer et al., 2018; Teichert et al., 2020;

source rock brines, we need to advance the scientific knowledge

on the origin, fate, and transport of Li. Here, the source rock brines

To determine the locations with high concentrations of Li in

Williams and Hervig, 2005; Williams et al., 2013).

E-mail address: kjlee6@central.uh.edu.

Nomenclature **Variables** A_k Frequency factor C^{κ} Concentration of component C_P Specific heat capacity Activation energy E_k h Specific enthalpy Reaction enthalpy Δh_k Ionic strength of aqueous solution Selectivity coefficient K_{AB} Reaction rate constant k_k Effective permeability k_{β} Activity coefficient of cation ν Diffusivity η Viscosity μ Density O Media porosity φ Vectors Gravity g **Jacobian** matrix J **Superscript** Component к **Subscripts** Ν Equivalent fractional occupancy Reaction rate r_k P Pressure R Gas constant R_i Residual equation Sensitivity coefficient S_{ii} Phase saturation S_{β} \overline{S}_{ii} Scaled sensitivity coefficient Τ Temperature Χ Mass fraction of component in phase X_i Primary variable Z Valence of cation Α Aqueous phase 0 Liquid organic phase G Gaseous phase geol Geologic time scale Order of equation i Order of variable i Kinetic reaction k R Rock S Solid phase Simulation time scale sim β Phase

and transport of elements and compounds, but researched the reaction mechanisms of kerogen conversion as a source of oil and gas, and failed to identify the potential of kerogen in releasing Li (Braun and Burnham, 1990; Curiale and Curtis, 2016). On the other hand, Li in geologic systems has been researched as a trace element in the discipline of geochemistry, which has lacked the capability of addressing the chemical reactions and hydrogeologic

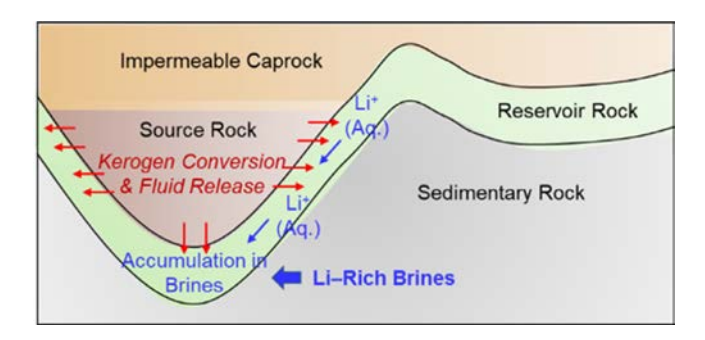


Fig. 1. A conceptual diagram of petroleum source rock system where Li-rich brines present.

phenomena relevant to the fate and transport of Li and failed to quantify the potential of Li production from petroleum source rock brines (Burton and Vigier, 2012; Pistiner and Henderson, 2003; Vigier et al., 2015).

To successfully secure Li from source rock brines, it is crucial to advance the knowledge and understanding of the origin, fate, and transport of Li, by combining the research focuses of petroleum engineering and geochemistry disciplines. In this regard, we set the purpose of this study as (1) to develop the advanced numerical simulation model that addresses the reaction mechanisms of kerogen releasing organic and inorganic elements including Li, transport of Li through permeable formation, and accumulation of Li in adjacent brines and (2) to evaluate the most influential factors affecting the concentration of Li, for the quantitative prediction of production potential of Li from petroleum source rock brines. We combine the local sensitivity analysis methodology with the developed numerical simulator to achieve the purpose of this study.

2. Development of basin-scale simulation model

2.1. Scientific background

Source rock brines occur at the subsurface formations deeper than 2 km, and their concentrations of Li are highly heterogeneous. In order to determine the locations of high concentrations of Li in source rock brines, it is critical to understand the entire physical and chemical phenomena relevant to the release of Li from its original source in source rocks, transport of released Li through connected pores, and accumulation of Li in brines. The original sources of Li can be either organic matter or inorganic minerals, given that organic matter called kerogen in source rock is recently found to release Li during its thermal maturation in geologic systems (Clauer et al., 2018; Williams et al., 2013).

Kerogen converts at high temperature above 150 °C, generating products including oil, gas, and inorganic elements including Li (Braun and Burnham, 1992; Carrie et al., 2012). Kerogen is categorized by its origin-Type I (lacustrine), Type II (marine), and Type III (terrestrial) (Tissot and Welte, 1984). When immature kerogen converts to organic and inorganic products, the maturity level of kerogen increases. Although the preceding researches on Li in kerogen-bearing petroleum source rocks are scarce, the published data on the relationship between total organic carbon (TOC, total concentration of kerogen and hydrocarbons) and solid Li in Green River Shale (immature Type I kerogen), Marcellus Shale (moderately mature Type II kerogen), and diverse oilfields (highly mature organic matters of various types) indicates the positive correlation between TOC and solid Li concentration (Table 1). As such, a significant amount of Li in petroleum source rock is released during kerogen maturation and transported into

Table 1Total Organic Carbon (TOC) and Li concentrations in diverse sedimentary formations.

Sedimentary formations TOC (wt%)		Li contents in solid phase (μg/g)
Green River Shale Marcellus Shale	1–33.7 (Feng, 2011; Katz, 1995) 1–11 (Song and Carr, 2020)	132.3-147 (Jochum et al., 2005) 7-48 (Phan et al., 2016)
Diverse oilfields*	1-6.9 (Hosterman, 1990)	2-18 (Hosterman, 1990)

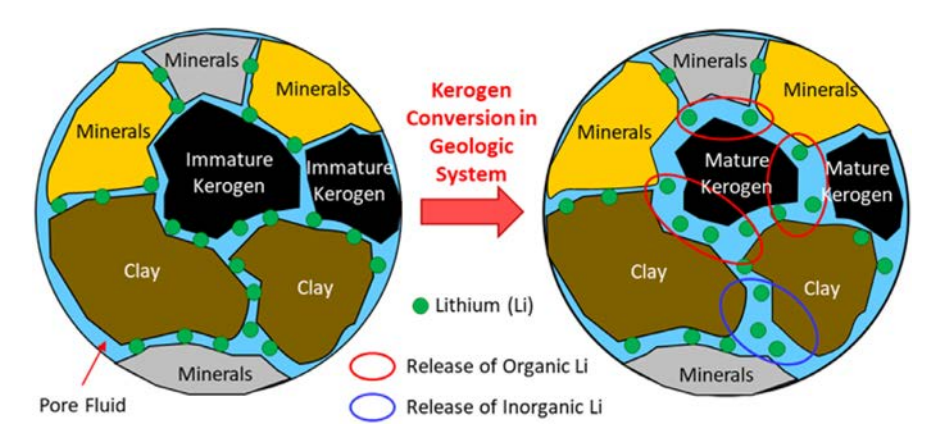


Fig. 2. A conceptual diagram of kerogen-bearing formation in pore-scale that undergoes kerogen conversion in geologic systems. Size of Li is exaggerated.

surrounding sediments. As can be seen in the conceptual diagram of kerogen-bearing formation that undergoes kerogen conversion, both organic and inorganic Li can be released by the solid kerogen decomposition and subsequent structural changes of minerals (Fig. 2).

Kerogen thermal maturation involves sequential and simultaneous kinetic reactions including solid kerogen decomposition, cracking of liquid oil into lighter hydrocarbons and residual carbons (pyrobitumen), cracking of hydrocarbon gas into lighter gases and pyrobitumens, and the decomposition of pyrobitumens into gases and different types of residual carbons (Braun and Burnham, 1990, 1992; Burnham and Braun, 2017; Burnham et al., 1987). They have been actively researched in the disciplines of petroleum engineering and petroleum geochemistry focusing on the potential of generating hydrocarbons and inorganic gases (such as carbon dioxide and hydrogen sulfide), but their potentials to release the mineral elements such as Li have not been determined yet (Behar et al., 2010, 1997; Craddock et al., 2015, 2017; Pepper and Corvi, 1995; Xiong et al., 2002). From Li isotope fractionation studies in kerogen-bearing shales in East Slovakian Basin and Baltic Basin, it has been found that organically bound ⁶ Li-enriched compounds are released into water during the thermal maturation of kerogen (Teichert et al., 2020; Williams et al., 2012; Williams and Hervig, 2005; Williams et al., 2013).

Released Li from kerogen thermal decomposition can accumulate in geologic systems either as immediately fixed on minerals or as dissolved in brines and transported. In the arid and highly alkaline environment with abundant clay, Li is well known to replace alkaline earth-metals and form Li-bearing smectite, or substitute into octahedral sites to form non-expandable illite (Burton and Vigier, 2012; Grosjean et al., 2012; Kesler et al., 2012; Kloprogge et al., 1999; Peiro et al., 2013; Penniston-Dorland et al., 2017; Starkey, 1982; Williams and Hervig, 2005). At the same time, the small ionic size of Li makes it easily dislodged from minerals through common cations as well as effortlessly dissolved in the brines of geologic systems (Vine, 1975). The ion chromatogram (Fig. 3) shows the detected cations in water, which has been leaching the powder samples of Green River Shale containing 30 vol%-kerogen at ambient pressure and temperature in our laboratory. The detection of Li cations in water suggests

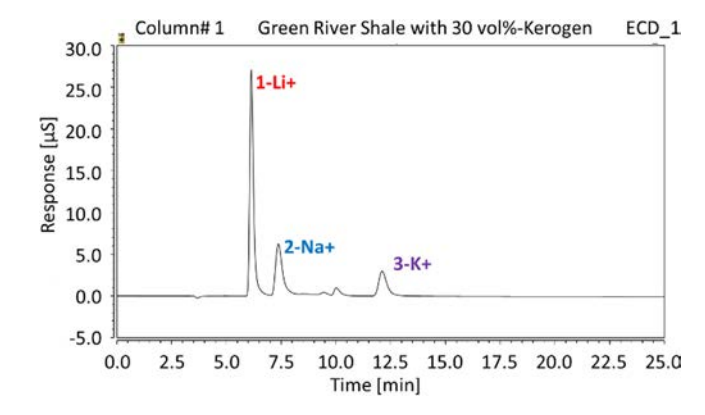


Fig. 3. Ion chromatogram. Condition—Isocratic mode; flow rate, 1.0 ml/min; MSA concentration, 29 mM; Dionex CS16 column; injection volume, 25 μ l; column temperature, 40 °C; suppression current, 44 mA.

the abundance of Li in kerogen-rich shale as well as an active exchange of Li between fluid and rock. Because clay minerals predominantly drive the mineralization and dissolution of Li, fraction of clay minerals will play a significant role in describing the transport of released Li.

2.2. Chemical reaction model and multicomponent–multiphase system

To describe the transport of released Li from kerogen thermal conversion in geologic systems, all the kinetic equations included in kerogen thermal maturation—kerogen decomposition releasing fluids and solids including Li, oil and gas cracking, and pyrobitumen decompositions—as well as the mineralization and dissolution of Li have been considered in the development of our numerical simulator (Tables 2 and 3). The numerical simulator includes 15 mass components of (1) water, (2) heavy oil (C24), (3) light oil (C9), (4) methane gas (C1), (5) mixed hydrocarbon gas (C3), (6) carbon dioxide (CO₂), (7) kerogen, (8–11) different types of residual carbons—pyrobitumen 1, pyrobitumen 2, pyrobitumen 3, and pyrobitumen 4, (12) Li ion (Li⁺), (13) Na ion (Na⁺, cation

Table 2Kinetic reactions of kerogen decomposition and subsequent decomposition of hydrocarbons and pyrobitumens (Braun and Burnham, 1992; Jochum et al., 2005).

Reactions	Frequency factor [1/s]	Activation energy [kJ/mol]	Reaction enthalpy [kJ/mol]
Kerogen \rightarrow 0.279 Heavy oil + 0.143 Light oil + 0.018 Hydrocarbon gas + 0.005	3.0×10^{13}	213.384	-335
Methane + 0.555 Pyrobitumen 1 + 1.41 \times 10 ⁻⁴ Li Heavy oil \rightarrow 0.373 Light oil + 0.156 Hydrocarbon gas + 0.03 Methane + 0.441 Pyrobitumen 2	1.0×10^{13}	225.936	-46.5
Light oil \rightarrow 0.595 Hydrocarbon gas + 0.115 Methane + 0.290 Pyrobitumen 3	5.0×10^{11}	225.936	-46.5
Hydrocarbon gas → 0.682 Methane + 0.318 Pyrobitumen 4	1.2×10^{12}	238.488	-46.5
Pyrobitumen 1 \rightarrow 0.031 Hydrocarbon gas + 0.033 Methane + 0.936 Pyrobitumen 2	1.0×10^{13}	225.936	-46.5
Pyrobitumen 2 \rightarrow 0.003 Hydrocarbon gas + 0.033 Methane + 0.964 Pyrobitumen 3	5.0×10^{11}	225.936	-46.5
Pyrobitumen 3 \rightarrow 0.018 Methane + 0.982 Pyrobitumen 4	1.2×10^{12}	238.488	-46.5

Table 3Cation exchange reaction between Li and Na.

Reaction (equilibrium)	Data taken into account in the model		
Na-clay + Li ⁺ ↔ Li-clay + Na ⁺	Selectivity coefficient for Li-Na exchange		

exchangeable with Li⁺), (14) Na–clay, and (15) Li–clay in four phases of aqueous, liquid organic, gaseous, and solid. Note that we considered Na ion as an exchangeable cation with Li ion through rock and fluid interactions. A representative example of clay is montmorillonite.

Kinetic reactions of decompositions of kerogen, hydrocarbons, and pyrobitumens in Table 2 are calculated based on the first-order Arrhenius law as follows. Subscript (k) indicates the order of reaction in Table 2.

$$r_k = k_k C^{\kappa} \tag{1}$$

where, r_k [kg/(m³ s)] is the reaction rate; C^{κ} [kg/m³] is the concentration of component; k_k [1/s] is the reaction rate constant, which is described as follows.

$$k_k = A_k \exp\left(-\frac{E_k}{RT}\right) \tag{2}$$

where, A_k [1/s] is the frequency factor; E_k [kJ/mol] is the activation energy; R [kJ/(mol K)] is the gas constant; T [K] is the system temperature.

Cation exchange reaction between Li and Na presented in Table 3 takes place when free cations in aqueous solution exchange with interlayer cations in clay. Selectivity coefficient for the cation exchange reaction is described as follows (Fernandes et al., 2012; Xu et al., 2008).

$$K_{AB} = \frac{(N_B)^{Z_A}}{(N_A)^{Z_B}} \frac{[A]^{Z_B}}{[B]^{Z_A}} \frac{(\gamma_A)^{Z_B}}{(\gamma_B)^{Z_A}}$$
(3)

where, K_{AB} is the selectivity coefficient (or equilibrium constant) for cation exchange reaction; Z_A and Z_B are the valences of cations A and B, respectively; N_A and N_B are the equivalent factional occupancies, defined as the equivalents of cations A and B adsorbed per kg of clay divided by the cation exchange capacity (CEC) [equiv/kg], respectively; [A] and [B] [M] are the molarities of cations A and B; γ_A and γ_B are the activity coefficients of cations A and A in aqueous solution, which are described as follows as per the modified Debye–Huckel formula (Davies and Shedlovsky, 1964; Liu et al., 2012).

$$-\log(\gamma_i) = \frac{0.529Z_i^2I^{0.5}}{1+I^{0.5}} \tag{4}$$

where, Z_i is the valence of the *i*-th cation; I [M] is the true ionic strength of the aqueous solution. From the experimental study on Li-Na exchange equilibrium in montmorillonite at T=298

K, it is found that the selectivity coefficient (K_{Na_li}) is in the range of 0.5058–0.7586 under the various initial conditions of pH, solution volumes, and concentrations, where the corresponding equilibrium coefficient $(\frac{[Li]}{[Na]}\frac{N'_{Na}}{N'_{Li}}, N'$ in [mol/g]) is in the range of 1.116–1.444 (Liu et al., 2012).

2.3. Governing equations and solution algorithm

Basin-scale simulation model considers porous media as continua, where each discretized element contains solid and fluid phases and has its own porosity. The capability of the numerical simulator for this study has been built by adding the capability of release, transport, and accumulation of Li into our 3-D Integral Finite Difference Method (IFDM) model for petroleum source rock systems, which has been developed based on the seed code of TOUGH2 of Lawrence Berkeley National Laboratory (Lee et al., 2014; Lee, 2014, 2019, 2020; Lee et al., 2018a,b, 2016a,b, 2017a,b; Moridis, 2012; Pruess et al., 1999). The numerical simulator solves a set of mass-and-energy balance equations, to address the release of Li from kerogen conversion, transport of Li as dissolved in aqueous phase, and accumulation of Li in source rock brines. As shown in the solution algorithm of Fig. 4, the simulator computes the fully-implicit solutions of a series of partial differential equations of mass-and-energy balance equations, after constructing the Jacobian matrix. Elaborating on physical interpretation of the mathematical formulations, the numerical simulator has the following details.

 Mass-balance equation addresses the mass accumulation by Darcy flow, source and sink, and mass change by the chemical reactions of kerogen conversion and cation exchange, as described as follows:

$$\frac{\partial C^{\kappa}}{\partial t} = \sum_{\beta \equiv A, O, G} q_{\beta} X_{\beta}^{\kappa} + \sum_{k \equiv reactions} M_{k}^{\kappa}
- \nabla \cdot \left(\sum_{\beta \equiv A, O, G} \frac{k_{\beta} \rho_{\beta}}{\mu_{\beta}} X_{\beta}^{\kappa} \left(\nabla P_{\beta} - \rho_{\beta} \mathbf{g} \right) \right)$$
(5)

Where, C^{κ} is the component concentrations [kg/m³]; t is the time [s]; q_{β} [kg/(m³ s)] is the source and sink term; X^{κ}_{β} is the mass fraction of component κ in phase β ; M^{κ}_{k} [kg/(m³s)] is the mass change of component κ through k-th reaction; k_{β} [m²] is the effective permeability of phase β ; μ_{β} [Pa s] is the viscosity of phase β ; ρ_{β} [kg/m³] is the density of phase β ; P_{β} [Pa] is the phase pressure; \mathbf{g} [m/s²] is the gravity vector. Solution of mass balance equations provides the spatial distributions of mass components including Li in each phase of fluids and solid.

 Energy-balance equation addresses the heat accumulation by heat conduction and convection, and heat change by chemical reactions, as described as follows:

$$\frac{\partial}{\partial t} \left((1 - \phi) \rho_R C_{P,R} T + \sum_{\beta \equiv A, O, G, S} \phi S_{\beta} \rho_{\beta} U_{\beta} \right)
= \nabla \cdot (K \nabla T) - \nabla \cdot \left(\sum_{\beta \equiv A, O, G} k \frac{k_{r\beta} \rho_{\beta}}{\mu_{\beta}} \left(\nabla P_{\beta} - \rho_{\beta} \mathbf{g} \right) h_{\beta} \right)
+ \sum_{k = positions} \Delta h_{k} r_{k}$$
(6)

Where, ϕ is the media porosity; ρ_R [kg/m³] is the dry rock density; $C_{P,R}$ [J/(kg K)] is the specific heat capacity of dry rock; T [K] is the temperature; S_β is the saturation of phase β ; U_β [J/kg] is the internal energy of phase β ; K [W/(m K)] is the thermal conductivity of bulk formation consisted of dry rock and the phases in pores; h_β [J/kg] is the specific enthalpy of phase β ; and Δh_k [J/kg] is the enthalpy of k-th kinetic reaction (see Table 2).

 Mass-and-energy-balance equations are simultaneously solved by computing the fully-implicit solution of Jacobian matrix, which is described as follows:

$$J = \left[\partial R_i / \partial X_i \right] \tag{7}$$

Where, J is the Jacobian matrix; R_i is the residual equations of mass-and-energy-balance equations; X_j is the primary variables such as P_{β} , X_{β}^{κ} , S_{β} , and T. The Jacobian matrix equation is solved by applying Newton–Raphson method.

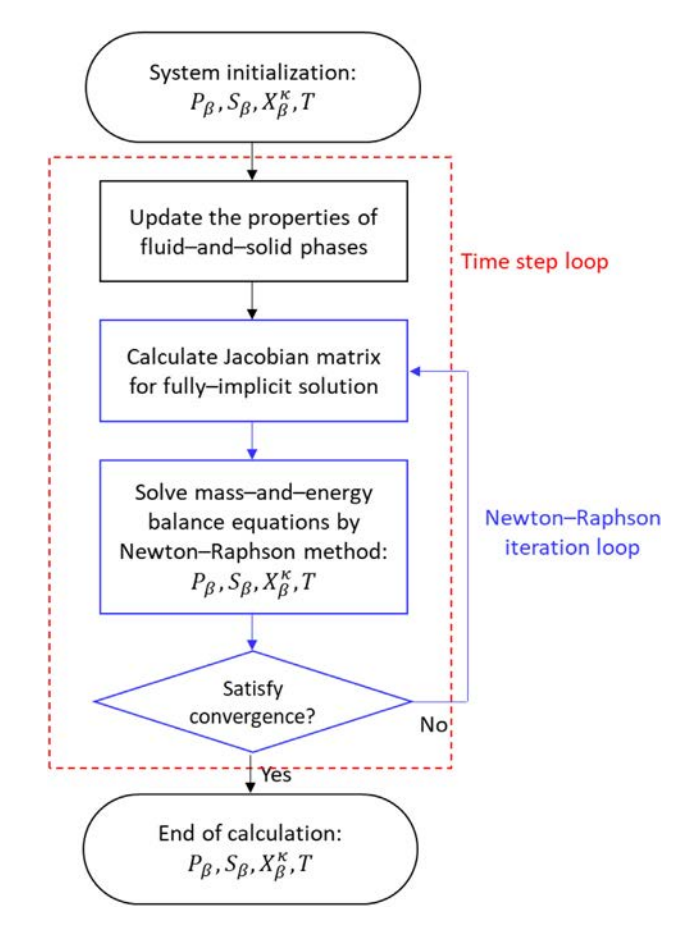
2.4. Dynamic system conditions affecting the release, transport, and accumulation of li

In the geologic systems, where kerogen releases organic and inorganic components during thermal conversion, and subsequent transport of them occurs, in-situ conditions such as pressure, temperature, and compositions and properties of phases undergo significant changes (Bauman and Deo, 2010; Fan et al., 2010; Youtsos et al., 2013). Changes of pressure and temperature accompanied by kerogen decompositions into fluid and solid affect phase behavior, such as liquefaction of gaseous phase, vaporization of liquid phase, and dissolution and escapement of gas components into and from liquid phase. Subsequently, thermophysical and chemical states of the fluid and solid phases affect the transport and accumulation of components including Li in the geologic systems. These dynamic system conditions relevant to release, fate, and transport of Li in entire petroleum systems have been addressed in this study's basin-scale simulation model. The description of dynamic phase properties such as density, viscosity, specific enthalpy, compositional thermal conductivity, and solubility are computed as a function of pressure, temperature, and phase compositions, by considering individual component's characteristics and mass fractions, mixing rules, and equation of states (Lee et al., 2016a).

3. Problem setup

3.1. Model geometry and input parameters

A 2D cross-sectional conceptual model of petroleum source rock system has been developed for the numerical simulation cases. The conceptual model includes the geometry of impermeable rock, source rock, and reservoir rock, with the simplified



 $\textbf{Fig. 4.} \ \ \textbf{Flow chart of the solution algorithm in the basin-scale simulation model}.$

representation of system heterogeneity. Although it is a simplified model, it includes the essential components affecting the release from kerogen, transport through the pores, and accumulation of Li in the entire petroleum source rock system. Numerical simulation cases with the conceptual model will provide the fundamental understanding of the physical and chemical phenomena relevant to the Li behavior by clearly analyzing the impact of various parameters affecting it. Fig. 5 shows the discrete grid geometry of the conceptual model, consisted with 60×30 cubic grids of $100 \text{ m} \times 100 \text{ m} \times 100 \text{ m}$. Release of Li from kerogen occurs in the source rock with high organic content (25 vol% of bulk rock), while its transport occurs in the reservoir rock with low organic content (2.5 vol% of bulk rock).

The system properties and initial conditions of the simulations are presented in Table 4. We consider the gradually increasing pressure and temperature with depth, based on the hydrostatic pressure gradient and geothermal gradient, respectively. Initial volume fraction of solid phase composed with the components of kerogen, pyrobitumens, Na-clay, and Li-clay were 25% in the entire domain; source rock had 25 vol%-kerogen with respect to bulk rock (corresponding mass fraction in solid phase of 1.0); reservoir rock had 2.64 vol%-kerogen, 21.1vol%-pyrobitumens, 0.63 vol%-Li-clay, and 0.63 vol%-Na-Clay with respect to bulk rock (corresponding mass fractions in solid phase of 0.1, 0.8, 0.05, and 0.05 for kerogen, pyrobitumens, Li-clay, and Na-clay, respectively); impermeable rock had 23.7 vol%-pyrobitumens, 0.63 vol%-Li-clay, and 0.63 vol%-Na-Clay with respect to bulk rock (corresponding mass fractions in solid phase of 0.9, 0.05, and 0.05 for pyrobitumens, Li-clay, and Na-clay, respectively). Note that the high value of TOC in the source rock has been obtained

Table 4System properties and initial conditions.

System properties and initial condition	Value
Pressure range, hydrostatic pressure gradient	3.04–32.4 MPa, 9,793 Pa/m
Temperature range, geothermal gradient	230-320 °C, 0.03 °C/m
Volume fraction of solid phase	25 vol%
Effective porosity	4 vol%
Na ion mass fraction in aqueous phase	1.0e-4
Na-Li equilibrium coefficient	1.2793
Li stoichiometry (mass fraction) in kerogen decomposition	1.41e-4

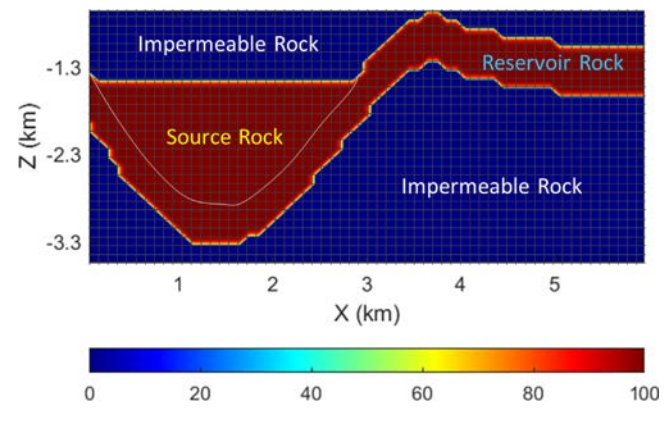


Fig. 5. Grid geometry and permeability [md] distribution of the 2D conceptual model containing different lithologic zones.

from the immature kerogen-bearing shale (Type I Green River Shale), instead of already matured kerogen-bearing shales with low TOC, given that we tried to address the release of Li from the maturation of initially immature kerogen during geological time-scale. As solid kerogen converts into organic and inorganic compounds in fluid and solid phases, the volume fractions of solid and pores go through dynamic changes. Initial effective porosity of entire domain was 4 vol%, where single phase aqueous phase presented initially. In the aqueous phase, 10^{-4} mass fraction of Na ion (Na⁺) presented initially in the pores. Equilibrium coefficient of Na-Li cation exchange between aqueous phase and clay minerals was 1.2793 as per the published value, where the corresponding selectivity coefficient was 0.6322 (Liu et al., 2012). Stoichiometry in mass fraction of Li released from the kerogen decomposition was assumed to be 1.41×10^{-4} , based on the solid Li fraction range in the immature kerogen-bearing shale (Table 1), and regarding that both organic and inorganic Li would be released by kerogen maturation in the geologic system (Fig. 2).

It is worthwhile to discuss the high temperature of initial condition (230-320 °C) in Table 4. Depth of the simulation model is from -300 m to -3300 m, which results in the actual formation temperature ($T_{\rm geol}$) of 30–120 °C. In the simulation runs, we considered the higher model temperature (T_{sim}) of 230–320 °C with the simulation time scale of multiple days, which had to be in a different scale from the actual geologic time scale (t_{geol}) of tens of millions of years. Kerogen decomposition at high temperature in simulation introduces the shorter simulation time (t_{sim}), by equating the multiplication of reaction rate constant and time in simulation scale (Eq. (8)) to that in geologic scale (Eq. (9)) and applying the kerogen decomposition kinetics in Table 2 (Pawar et al., 2017). As such, maximum simulation time of 2.31 days $(=2.0 \times 10^5 \text{ s})$ was found to be sufficient to consider the geologic time of about 10 My. Shorter simulation time scale affects the fluid flow as well, and diffusivity of fluid phases has been corrected, by considering the original shale permeability of nD scale (Eqs. (10) and (11)). Here, η_{geol} and η_{sim} indicate the diffusivity of fluid phase in geological time scale and simulation time scale,

respectively. Accordingly, absolute permeability of source rock and reservoir rock, which are both composed of low-permeability shale in petroleum source rock system, has been assigned to be 100 md in the simulation runs (Table 5).

$$k_{k,\text{geol}} \cdot t_{\text{geol}} = A_k \exp\left(-\frac{E_k}{RT_{\text{geol}}}\right) \cdot t_{\text{geol}}$$
 (8)

$$k_{k,\text{sim}} \cdot t_{\text{sim}} = A_k \exp\left(-\frac{E_k}{RT_{\text{sim}}}\right) \cdot t_{\text{sim}}$$
 (9)

$$\eta_{\text{geol}} \cdot t_{\text{geol}} = \frac{K_{\text{geol}}}{\varnothing \mu c_t} \cdot t_{\text{geol}}$$
(10)

$$\eta_{\text{sim}} \cdot t_{\text{sim}} = \frac{K_{\text{sim}}}{\varnothing \mu c_t} \cdot t_{\text{sim}} \tag{11}$$

3.2. Sensitivity analysis

We combine the local sensitivity analysis technique to the modeling of Li in petroleum source rock systems with the developed simulator, to quantitatively evaluate the most influential factors affecting the Li concentration in brines. Local sensitivity analysis was conducted by applying the simulation-optimization framework of iTOUGH2 with the PEST protocol, which was used to link our developed numerical simulator to the iTOUGH2 analysis toolset of Lawrence Berkeley National Laboratory (Finsterle, 1999, 2010). Local sensitivity analysis quantifies the relationship between unknown input parameters to the uncertain output variables.

In this study, the uncertain output variable has been defined as Li mass fraction in brines, while the unknown input parameters have been defined as the factors affecting release. transport, and accumulation of Li, such as Li stoichiometry in kerogen decomposition reaction, Na-Li equilibrium coefficient of cation exchange reaction between brines and clay minerals, initial Na-clay mass fraction in solid phase, initial Li-clay mass fraction in solid phase, and initial Na ion mass fraction in brines. These input parameters have been selected by considering their expected impacts on the Li mass fraction in brines (Table 6). Increase of Li stoichiometry in kerogen decomposition reaction is expected to positively affect the output variable by allowing more amount of Li releasable during kerogen decomposition into pore fluids. The other parameters are selected to analyze the impacts of rock and fluid interactions exchanging components during the transport of released Li through pores; increase of Na-Li equilibrium coefficient is expected to make the forward reaction of cation exchange in Table 3 more vigorous and enhance the Li mineralization; increase of Na-clay mass fraction in solid phase is expected to make the forward reaction of cation exchange and Li mineralization more active as well; increase of Li-clay mass fraction in solid phase is expected to make the backward reaction of cation exchange and Li dissolution more active; increase of Na ion mass fraction in brines is expected to enhance the backward reaction of cation exchange and Li dissolution as well.

Table 5 Formation properties of each zone.

Zone	Permeability [md]	Solid phase compositions (mass fractions)
In a second la made	0	$X_S^{Kerogen} = 0, X_S^{Cokes} = 0.9,$
Impermeable rock	0	$X_S^{Li-clay} = 0.05, X_S^{Na-clay} = 0.05$
Course made (shale with high oursein matter content)	100	$X_S^{Kerogen} = 1.0, X_S^{Cokes} = 0,$
Source rock (shale with high organic matter content)	100	$X_S^{Li-clay} = 0, X_S^{Na-clay} = 0$
Decoming week (abole with less engagin metter content)	100	$X_S^{Kerogen} = 0.1, X_S^{Cokes} = 0.8,$
Reservoir rock (shale with low organic matter content)	100	$X_S^{Li-clay} = 0.05, X_S^{Na-clay} = 0.05$

Table 6Expected impacts of input parameters on the output variable and the scaling factors (variations of parameters and standard deviation of output variable) for local sensitivity analysis.

Input parameters and output variable	Expected impact	Scaling factor
Input parameter: Li stoichiometry in kerogen decomposition reaction	Positive	2.82e-6
Input parameter: Na-Li equilibrium coefficient	Negative	2.5586e-2
Input parameter: Na-clay mass fraction in solid phase	Negative	1.0e-3
Input parameter: Li-clay mass fraction in solid phase	Positive	1.0e-3
Input parameter: Na ion mass fraction in brines	Positive	2.0e-6
Output variable: Li ion mass fraction in brines	-	1.0e-6

In the local sensitivity analysis, sensitivity coefficient is computed as follows, which is defined as the partial derivatives of output variables to input parameters.

$$S_{ij} = \frac{\partial Z_i}{\partial P_i} \tag{12}$$

Where, S_{ij} is the sensitivity coefficient of output variable (Z_i) to the input parameter (P_j) . Because the variability of input parameters and the uncertainty of output variables vary, scaled sensitivity coefficients are computed to make the sensitivity coefficients dimensionless, as described as the following equation.

$$\bar{S}_{ij} = \frac{\partial Z_i}{\partial P_i} \cdot \frac{\sigma P_j}{\sigma Z_i} \tag{13}$$

Where, \overline{S}_{ij} is the scaled sensitivity coefficient of output variable (Z_i) to the input parameter (P_j) ; σP_j is the parameter scaling factor, which is defined by the expected variability of input parameter; σZ_i is the output scaling factor, which is defined by the uncertainty or standard deviation of output variable. The scaling factors of input parameters and output variable applied in this study are presented in Table 6, which are assumed to be around 2% of each parameter and expected variable.

4. Results and discussion

4.1. basin-scale modeling

We simulated the processes of kerogen decomposition releasing Li, transport of released Li through pores as dissolved in brines, and accumulation of Li in petroleum source rock systems, as discussed in Section 3.1 Model geometry and input parameters. Fig. 6(a) presents the spatial distributions of mass fraction of Li in brines after the simulation time of 2.0×10^5 s in the base case, by applying the system properties and initial conditions presented in Tables 4 and 5. Note that we presented the spatial distributions of mass fraction of Li in brines instead of its concentration in ppm, because mass fraction in fluid phase indicates the relative amount of the component in the in-situ condition of reservoir, while the concentration in ppm is generally used at the surface standard condition. From the figures, it is found that the part of the Li released from kerogen was expelled from source rock and transported through the pores of reservoir rock and accumulated, while significant part of Li released from kerogen was staying and

accumulated in source rock. Table 7 shows the Li mass fraction in brines at the various observation points of 1 (x = 1.5 km, z = -1.8 km), 2 (x = 1.5 km, z = -2.4 km), 3 (x = 1.5 km, z = -2.4 km) -3.0 km), and 4 (x = 5.5 km, z = -1.3 km). Li mass fractions in brines at the observation points 1, 2, 3, and 4 accordingly indicate the Li concentration of 76.2 ppm, 430 ppm, 191 ppm, and 19.1 ppm, respectively, at surface standard condition of 1 atm pressure and 25 °C temperature. The magnitudes of these Li concentrations are in accordance with the published values in Li-rich source rock brines, which give us confidence in our developed simulator and the conditions of simulation-scale time and diffusivity (Haluszczak et al., 2013; Jang et al., 2017; Jang and Chung, 2018). More specifically, upstream chain suppliers, who produce oil and gas from source rocks, reported that water produced from Marcellus Shale contains Li from tens to a few hundreds ppm (Jang et al., 2017; Pfister et al., 2017; Phan et al.,

Prior to the local sensitivity analysis of the Li mass fraction in brines, various parameters were tested to directly quantify their impacts. Fig. 6(b)-(f) show the spatial distributions of Li mass fractions in brines after the simulation time of 2.0×10^5 s in the cases 1, 2, 3, 4, and 5. Case 1 indicates the case of increased Li stoichiometry from kerogen decomposition (base case: 1.41×10^{-4} , case 1: 2.82×10^{-4}); case 2 indicates the case of increased equilibrium coefficient of Na-Li cation exchange reaction (base case: 1.2793, case 2: 2.5586); case 3 indicates the case of increased initial mass fraction of Na-clay in reservoir rock (base case: 0.05, case 3: 0.10); case 4 indicates the case of increased initial mass fraction of Li-clay in reservoir rock (base case: 0.05, case 4: 0.10); case 5 indicates the case of increased initial mass fraction of Na ion in brines (base case: 10^{-4} , case 5: 2×10^{-4}). In each case, the other system properties and initial conditions were identical to the base case. As can be seen in Fig. 6(b), increased Li stoichiometry from kerogen decomposition (case 1) positively affected the Li mass fraction in brines in source rock, reservoir rock under the source rock, and reservoir rock besides the source rock. Increased equilibrium coefficient of Na-Li cation exchange reaction (case 2) and increased initial mass fraction of Na-clay in reservoir rock (case 3) did not affect the Li mass fraction in brines in source rock, while they negatively affected them in reservoir rocks under and besides the source rock (Fig. 6(c) and (d)). Increased initial mass fraction of Liclay in reservoir rock had insignificant impact on the Li mass fraction in brines in source rock, while it positively affected them

Table 7Li mass fractions in brines (and Li concentration in ppm at surface condition) at the end of the simulations.

Observation points in various locations	Base case	Case 1	Case 2	Case 3	Case 4	Case 5
Observation point 1 (x = 1.5 km, z = -1.8 km)	6.0691e-5	1.2138e-4	6.0691e-5	6.0367e-5	6.0367e-5	6.0689e-5
	(76.2 ppm)	(152 ppm)	(76.2 ppm)	(75.8 ppm)	(75.8 ppm)	(76.2 ppm)
Observation point 2 $(x = 1.5 \text{ km}, z = -2.4 \text{ km})$	3.5716e-4	7.1421e-4	3.5716e-4	3.5727e-4	3.5726e-4	3.5715e-4
	(430 ppm)	(860 ppm)	(430 ppm)	(430 ppm)	(430 ppm)	(430 ppm)
Observation point 3 $(x = 1.5 \text{ km}, z = -3.0 \text{ km})$	1.5515e-4	3.0172e-4	1.0230e-4	1.0857e-4	2.2510e-4	1.6850e-4
	(192 ppm)	(372 ppm)	(126 ppm)	(133 ppm)	(276 ppm)	(208 ppm)
Observation point 4 $(x = 5.5 \text{ km}, z = -1.3 \text{ km})$	1.5232e-5	1.6946e-5	9.8366e-6	9.8942e-6	2.1136e-5	2.8708e-5
	(19.2 ppm)	(21.3 ppm)	(12.3 ppm)	(12.4 ppm)	(26.5 ppm)	(36 ppm)

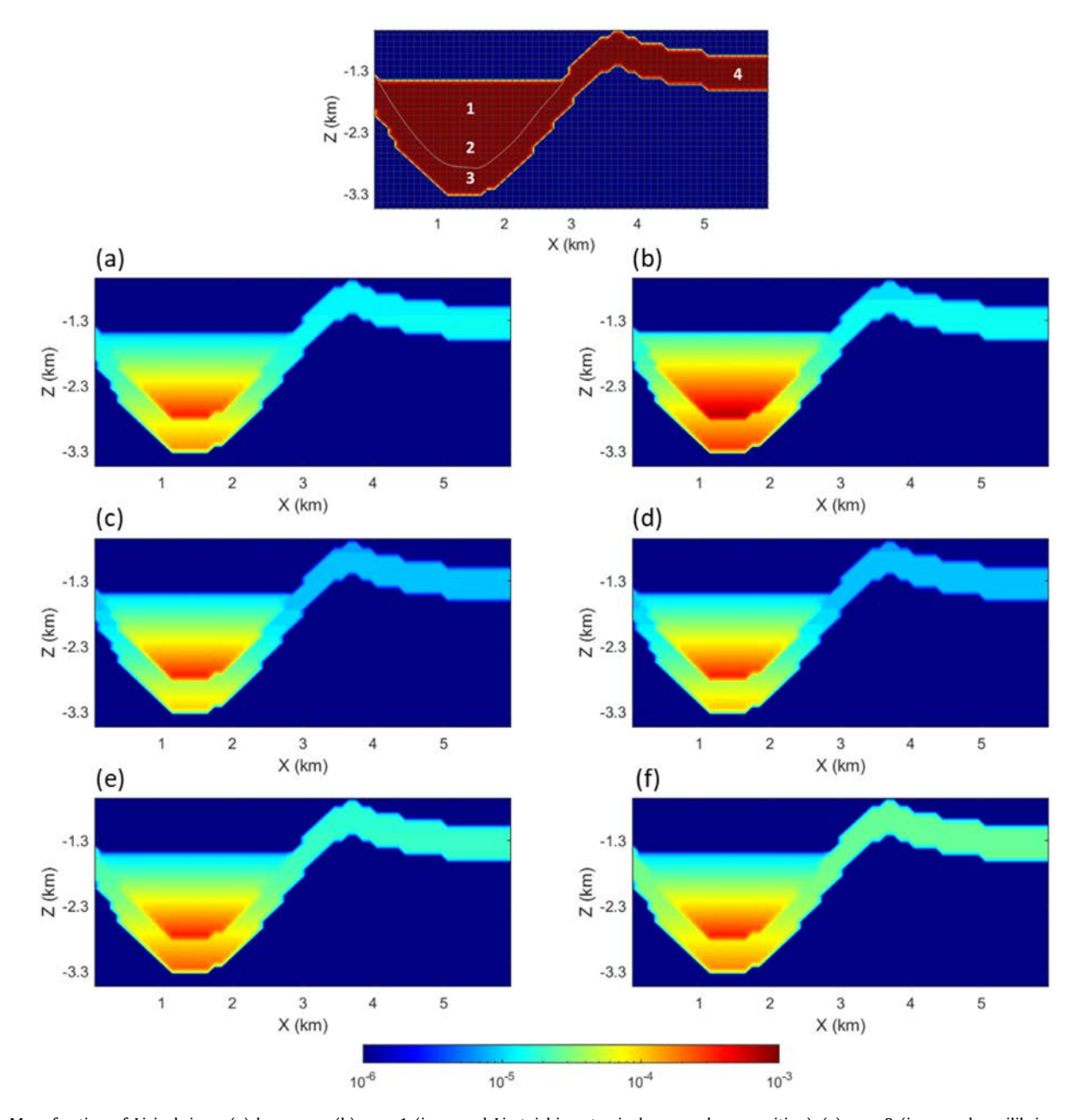


Fig. 6. Mass fraction of Li in brines—(a) base case, (b) case 1 (increased Li stoichiometry in kerogen decomposition), (c) case 2 (increased equilibrium coefficient of Na–Li cation exchange reaction), (d) case 3 (increased initial mass fraction of Na–clay in reservoir rock), (e) case 4 (increased initial mass fraction of Li–clay in reservoir rock), (f) case 5 (increased initial mass fraction of Na ion in brines).

Table 8Li mass in place as dissolved in brines at the end of the simulations.

Case	Li mass in place (kg)	Normalized Li mass in place to the base case
Base case	8.0253×10^5	-
Case 1-increased Li stoichiometry in kerogen decomposition	1.4815×10^{6}	1.8460
Case 2-increased equilibrium coefficient of Na-Li cation exchange reaction	6.9346×10^{5}	0.8641
Case 3-increased initial mass fraction of Na-clay in reservoir rock	7.0104×10^5	0.8735
Case 4-increased initial mass fraction of Li-clay in reservoir rock	9.3521×10^5	1.1653
Case 5—increased initial mass fraction of Na ion in brines	9.2934×10^5	1.1580

in reservoir rocks under and besides the source rock (Fig. 6(e)). Finally, increased initial mass fraction of Na ion in brines (case 5) had insignificant impact on the Li mass fraction in brines in source rock, while it positively affected them in reservoir rocks under and besides the source rock (Fig. 6(f)). Impacts of increased initial mass fraction of Li-clay in reservoir rock (case 4) and increased initial mass fraction of Na ion in brines (case 5) were in a similar pattern, but they showed different relative impacts on the Li mass fractions in the reservoir rocks, which were under and besides the source rock brines. Table 7 shows the Li mass fraction in brines at the various observation points in each case. These results indicate that the various parameters differently affect the Li mass fraction in brines with respect to the location in the system, which are resulted by the combined effects of release and transport of Li and rock and fluid interactions. It raises the need of analyzing the impacts of various parameters at different observation points to quantify the most influential factors, which would vary with locations.

In Table 8, generated mass in place (kg) of Li in brines is summarized in the base case and each case of various parameters. With the same degree (two times) of increase in each input parameter, it is found that the impact of Li stoichiometry in kerogen decomposition had the highest sensitivity of the generated Li amount in brines in the entire system, where the impacts of initial mass fraction of Li–clay in reservoir rock, initial mass fraction of Na ion in brines, initial mass fraction of Na–clay in reservoir rock, and equilibrium coefficient of Na–Li cation exchange reaction followed it.

4.2. Impacts of kerogen type and content

Before performing the local sensitivity analysis as stated, the impacts of kerogen types and contents on Li mass fraction in brines were estimated. Note that different kerogen types and contents were not considered in the local sensitivity analysis in the next section, because originally immature kerogen-bearing shale (Type I Green River Shale) with high TOC was considered, instead of already matured kerogen-bearing shales with low TOC, given that we tried to address the release of Li from the maturation of initially immature kerogen during geological time-scale. Regarding that activation energy of kerogen varies with respect to its maturity and type, we conducted two different simulation runs with (1) higher activation energy of kerogen decomposition (=214.384 kJ/mol) and with (2) lower kerogen volume fraction (=20 vol%).

Fig. 7 presents the spatial distributions of mass fraction of Li in brines after the simulation time of 2.0×10^5 s in the base case (activation energy of kerogen decomposition = 213.384 kJ/mol, kerogen volume fraction = 25 vol%) and the cases with increased activation energy of kerogen decomposition and decreased kerogen volume fraction. In Table 9, generated mass in place (kg) of Li in brines is quantitatively summarized in each case. Both cases show the negative impact on the mass fraction of Li in brines.

4.3. Sensitivity analysis

We performed a local sensitivity analysis of Li mass fraction in brines at the four observation points to the factors affecting release, transport, and accumulation of Li. The four observation points were set identical to the previous section of forward numerical simulation—observation points of 1 (x = 1.5 km, z =-1.8 km), 2 (x = 1.5 km, z = -2.4 km), 3 (x = 1.5 km, z = 1.5= -3.0 km), and 4 (x = 5.5 km, z = -1.3 km). Various input parameters such as Li stoichiometry in kerogen decomposition reaction, Na-Li equilibrium coefficient of cation exchange reaction between brines and clay minerals, initial Na-clay mass fraction in solid phase, initial Li-clay mass fraction in solid phase, and initial Na ion mass fraction in brines were selected to perturb in the local sensitivity analysis. After perturbing these parameters, corresponding changes in Li mass fraction in brines at the four observation points were monitored. By conducting the forward numerical simulations combined with the local sensitivity analysis using the scaling factors in Table 6, the summated absolute scaled sensitivity coefficients of Li mass fraction in brines to the various parameters have been obtained. The scaled sensitivity coefficients were obtained from $t = 10^4$ s to 2×10^5 s with a measurement frequency of 10⁴ s. For each parameter and output response of Li mass fraction in brines at each observation point, the summated absolute scaled sensitivity coefficients were computed as follows.

$$\overline{S}_{ij,sum} = \sum_{\text{for all } t} |\overline{S}_{ij}| \tag{14}$$

As can be seen in Table 10, each observation point had different sensitivity to the various input parameters. At the observation point 1 in the source rock, output response (Li mass fraction in brines) had the highest sensitivity to the Li stoichiometry in kerogen decomposition reaction and the insignificant sensitivity to the other parameters. At the observation point 2 in the deeper formation of source rock, output response showed much higher sensitivity to the Li stoichiometry than the observation 1, while the other input parameters remained insignificant. At the observation point 3 at the reservoir rock below the source rock, output response showed the high sensitivity to all the parameters, indicating that it was crucially affected by all the parameters relevant to the release and transport of Li. At the observation point 4 at the reservoir rock besides the source rock, output response had the higher sensitivity to the parameters affecting the transport of Li than the parameter affecting the release of Li from kerogen decomposition. The results in Table 10 are visually described in Fig. 8. As such, the presented results of local sensitivity analysis can provide the conceptual information of most important parameters to be investigated to quantitatively predict the Li production potential from brines at various locations in the petroleum source rock systems.

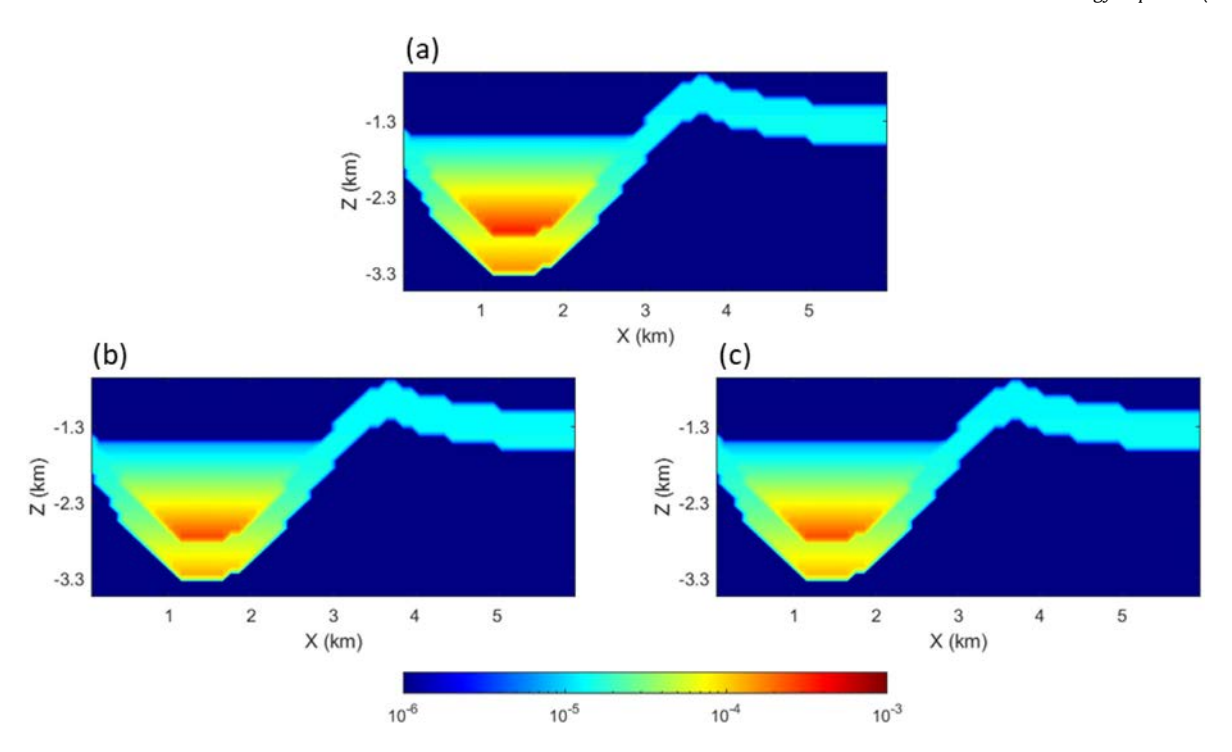


Fig. 7. Mass fraction of Li in brines—(a) base case, (b) case I (increased activation energy of kerogen decomposition), (c) case II (decreased initial kerogen content).

Table 9
Li mass in place as dissolved in brines at the end of the simulations.

Case	Li mass in place (kg)	Normalized Li mass in place to the base case
Base case	8.0253×10^5	-
Case I-increased activation energy of kerogen decomposition	6.5306×10^5	0.8138
Case II-decreased initial kerogen content	6.4064×10^5	0.7983

Table 10Scaled sensitivity coefficients of Li mass fraction in brines to the factors affecting release, transport, and accumulation of Li.

Scaled sensitivity coefficients of Li mass fraction in brines to various parameters	Li stoichiometry	Na–Li equilibrium coefficient	Na-clay fraction ^a	Li-clay fraction ^a	Na ion fraction ^a
Observation point 1 (x = 1.5 km, z = -1.8 km)	12.3384	0	0.0002	0.0002	-0.0002
Observation point 2 (x = 1.5 km, z = -2.4 km)	65.7752	0	0.031	0.031	-0.0002
Observation point 3 (x = 1.5 km, z = -3.0 km)	29.5952	-17.9416	-16.1716	19.7546	5.3638
Observation point 4 (x = 5.5 km, z = -1.3 km)	0.3620	-3.1534	-3.1314	3.1790	5.4000

^aFractions of Na-clay and Li-clay are the mass fractions in solid phase; fraction of Na ion is the mass fraction in brines.

5. Conclusions

In this study, we investigated the production potential of Li from petroleum source rock brines and quantified the impacts of various parameters relevant to the release, transport, and accumulation of Li on its production potential. The subject matter was addressed by means of basin-scale numerical simulation and local sensitivity analysis.

The numerical simulation with a conceptual model of petroleum source rock system addressed the accumulation of Li in various locations, by taking account for the release of Li from kerogen decomposition reaction in organic-rich source rock, and fate and transport of expelled Li as interacting with reservoir rock. From the simulation results, we could quantitatively analyze the Li mass fraction in brines as an indicator of Li production potential. In combination with the numerical simulations, we quantified the impacts of various parameters on the Li mass fraction in brines at four different observation points, by conducting local sensitivity analysis. It elucidated the relative sensitivity of Li production potential to the parameters of Li stoichiometry in

kerogen decomposition reaction, Na–Li equilibrium coefficient, Na–clay mass fraction in solid phase, Li–clay mass fraction in solid phase, and Na ion mass fraction in brines.

Specifically, the following detailed results were drawn:

- (1) In the numerical simulation of base case, Li concentrations at the upper part of the source rock (observation point 1), lower part of the source rock (observation point 2), reservoir rock below the source rock (observation point 3), and reservoir rock besides the source rock (observation point 4) were 76.2 ppm, 430 ppm, 191 ppm, and 19.1 ppm, respectively. These values are in accordance with the published values in Li–rich source rock brines and gave us confidence in our developed numerical simulator and the system conditions.
- (2) Two times-increment of Li stoichiometry in kerogen decomposition reaction, Na-Li equilibrium coefficient, Naclay mass fraction in solid phase, Li-clay mass fraction in solid phase, and Na ion mass fraction in brines resulted in the normalized Li mass in place as dissolved in brines to

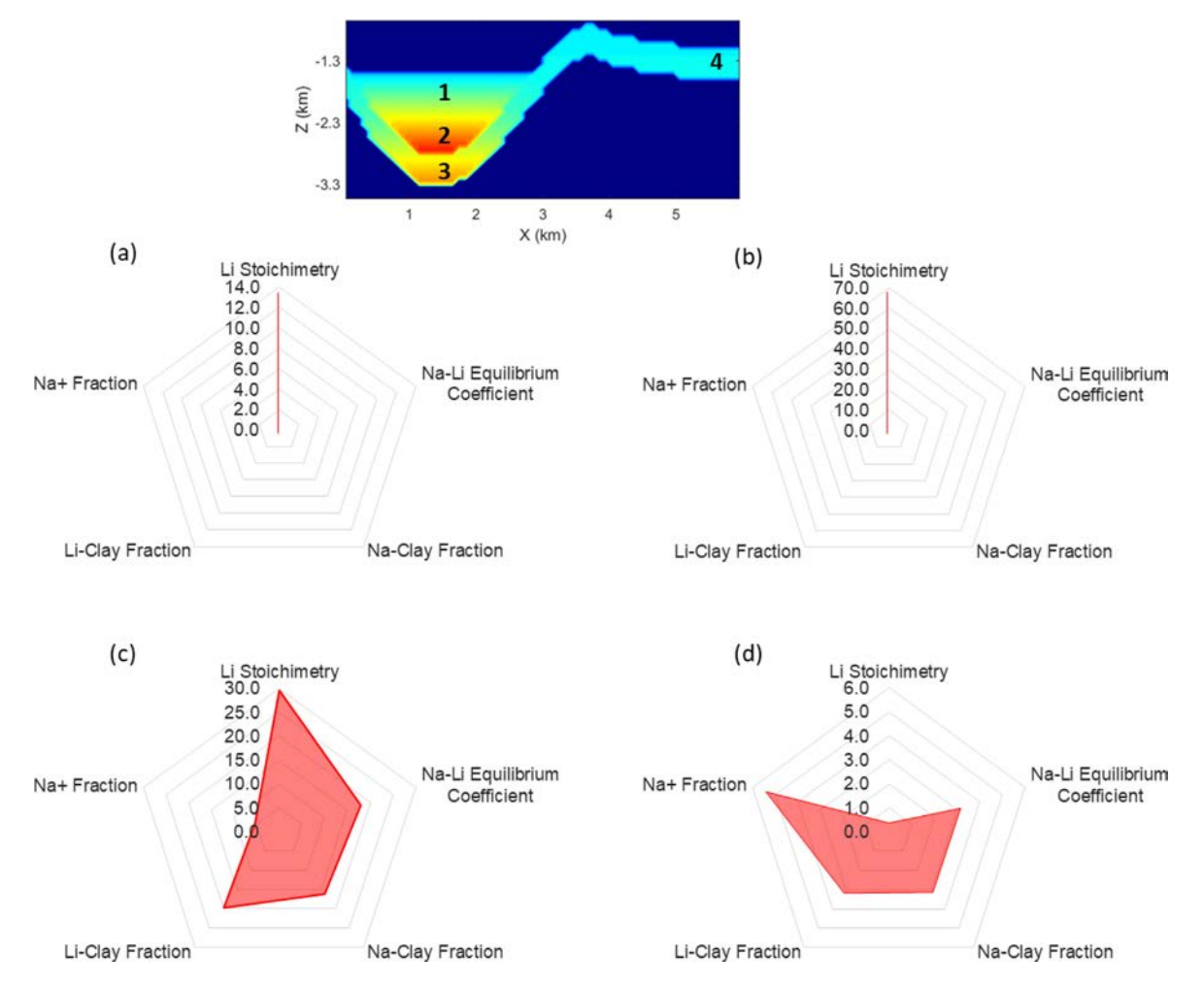


Fig. 8. Scaled sensitivity coefficients of Li mass fraction in brines to the various factors affecting release, transport, and accumulation of Li—(a) observation point 1, (b) observation point 2, (c) observation point 3, (d) observation point 4.

the base case of 1.8460, 0.8641, 0.8735, 1.1653, and 1.1580, respectively.

- (3) In the local sensitivity analysis, it is found that the Li mass fractions in brines at the source rock (observation points 1 and 2) were only affected by the Li stoichiometry in kerogen decomposition reaction and not affected by the other parameters. At the reservoir rock below the source rock (observation point 3), Li stoichiometry in kerogen decomposition reaction showed the highest sensitivity, and the other parameters (Na-Li equilibrium coefficient, Naclay mass fraction in solid phase, Li-clay mass fraction in solid phase, and Na ion mass fraction in brines) showed high sensitivities as well. At the reservoir rock besides the source rock (observation point 4), Na ion mass fraction in brines showed the highest sensitivity, where Li-clay mass fraction in solid phase, Na-Li equilibrium coefficient, Naclay mass fraction in solid phase, and Li stoichiometry in kerogen decomposition reaction followed it.
- (4) Among the various parameters, Li stoichiometry in kerogen decomposition reaction had the most significant impact on Li production potential, when it was summed at all of the four observation points, which was followed by Li–clay mass fraction in solid phase, Na–Li equilibrium coefficient, Na–clay mass fraction in solid phase, and Na ion mass fraction in brines. Among the various locations in the system, Li production potential at the reservoir rock below the source

rock (observation point 3) showed the highest sensitivity to the parameters, where lower part of the source rock (observation point 2), reservoir rock besides the source rock (observation point 4), and the upper part of the source rock (observation point 1) followed it.

The envisioned work will include the application of complex model geometries in numerical simulations, mimicking actual petroleum source rock systems with the consideration of specific lithologic structures and heterogeneity of system properties.

CRediT authorship contribution statement

Kyung Jae Lee: Conception and design, Development of numerical simulator, Conduction of experiment, Analysis and interpretation of the data, Writing and edition of text, Visualization, Funding acquisition, Resources, Project administration.

Declaration of competing interest

The authors declare that they have no known competing financial interests or personal relationships that could have appeared to influence the work reported in this paper.

Acknowledgments

The author appreciates the funding for this research from National Science Foundation, United States under Award 2042504

(CAREER: Identifying a New Source of Lithium for Sustainable and Renewable Energy Storage).

References

- Bauman, J.H., Deo, M.D., 2010. Parameter space reduction and sensitivity analysis in complex thermal subsurface production processes. Energy Fuels 25 (1), 251–259.
- Behar, F., Roy, S., Jarvie, D., 2010. Artificial maturation of a Type I kerogen in closed system: Mass balance and kinetic modelling. Org. Geochem. 41 (11), 1235–1247.
- Behar, F., Vandenbroucke, M., Tang, Y., Marquis, F., Espitalie, J., 1997. Thermal cracking of kerogen in open and closed systems: determination of kinetic parameters and stoichiometric coefficients for oil and gas generation. Org. Geochem. 26 (5–6), 321–339.
- Braun, R.L., Burnham, A.K., 1990. Mathematical model of oil generation, degradation, and expulsion. Energy Fuels 4 (2), 132–146.
- Braun, R.L., Burnham, A.K., 1992. PMOD: a flexible model of oil and gas generation, cracking, and expulsion. Org. Geochem. 19 (1-3), 161-172.
- Burnham, A.K., Braun, R.L., 2017. Simple relative sorptivity model of petroleum expulsion. Energy Fuels 31 (9), 9308–9318.
- Burnham, A.K., Braun, R.L., Gregg, H.R., Samoun, A.M., 1987. Comparison of methods for measuring kerogen pyrolysis rates and fitting kinetic parameters. Energy Fuels 1 (6), 452–458.
- Burton, K., Vigier, N., 2012. Lithium isotopes as tracers in marine and terrestrial environments. In: Handbook of Environmental Isotope Geochemistry. Springer, pp. 41–59.
- Carrie, J., Sanei, H., Stern, G., 2012. Standardisation of rock-eval pyrolysis for the analysis of recent sediments and soils. Org. Geochem. 46, 38-53.
- Clauer, N., Williams, L.B., Lemarchand, D., Florian, P., Honty, M., 2018. Illitization decrypted by B and Li isotope geochemistry of nanometer-sized illite crystals from bentonite beds, East Slovak Basin. Chem. Geol. 477, 177–194.
- Craddock, P.R., Prange, M., Pomerantz, A.E., 2017. Kerogen thermal maturity and content of organic-rich mudrocks determined using stochastic linear regression models applied to diffuse reflectance IR Fourier transform spectroscopy (DRIFTS). Org. Geochem..
- Craddock, P.R., et al., 2015. Evolution of kerogen and bitumen during thermal maturation via semi-open pyrolysis investigated by infrared spectroscopy. Energy Fuels 29 (4), 2197–2210.
- Curiale, J.A., Curtis, J.B., 2016. Organic geochemical applications to the exploration for source-rock reservoirs—a review. J. Unconv. Oil Gas Resour. 13, 1–31.
- Davies, C.W., Shedlovsky, T., 1964. Ion association. J. Electrochem. Soc. 111 (3), 85.
- Fan, Y., Durlofsky, L., Tchelepi, H.A., 2010. Numerical simulation of the in-situ upgrading of oil shale. SPE J. 15 (02), 368–381.
- Feng, J., 2011. Source Rock Characterization of the Green River Oil Shale, Piceance Creek Basin, Colorado. Colorado School of Mines, Arthur Lakes Library.
- Fernandes, M.M., Baeyens, B., Beaucaire, C., 2012. Radionuclide retention at mineral-water interfaces in the natural environment. In: Radionuclide Behaviour in the Natural Environment. Elsevier, pp. 261–301.
- Finsterle, S., 1999. ITOUGH2 User's Guide, LBNL-40040. p. 130.
- Finsterle, S., 2010. ITOUGH2 Universal Optimization using the PEST Protocol, User's Guide. Lawrence Berkeley National Laboratory, Berkeley, USA.
- Gielen, D., et al., 2019. The role of renewable energy in the global energy transformation. Energy Strategy Rev. 24, 38–50.
- Grosjean, C., Miranda, P.H., Perrin, M., Poggi, P., 2012. Assessment of world lithium resources and consequences of their geographic distribution on the expected development of the electric vehicle industry. Renew. Sustain. Energy Rev. 16 (3), 1735–1744.
- Haluszczak, L.O., Rose, A.W., Kump, L.R., 2013. Geochemical evaluation of flow-back brine from Marcellus gas wells in Pennsylvania, USA. Appl. Geochem. 28, 55–61.
- Hosterman, J.W., 1990. Chemistry and Mineralogy of Natural Bitumens and Heavy Oils and their Reservoir Rocks from the United States, Canada, Trinidad and Tobago, and Venezuela, 1047. US Government Printing Office.
- Jang, Y., Chung, E., 2018. Adsorption of lithium from shale gas produced water using titanium based adsorbent. Ind. Eng. Chem. Res. 57 (25), 8381–8387.
- Jang, E., Jang, Y., Chung, E., 2017. Lithium recovery from shale gas produced water using solvent extraction. Appl. Geochem. 78, 343–350.
- Jochum, K.P., et al., 2005. GeoReM: a new geochemical database for reference materials and isotopic standards. Geostand. Geoanal. Res. 29 (3), 333–338.
- Katz, B., 1995. The Green River Shale: an Eocene carbonate lacustrine source rock. In: Petroleum Source Rocks. Springer, pp. 309–324.
- Kesler, S.E., et al., 2012. Global lithium resources: Relative importance of pegmatite, brine and other deposits. Ore Geol. Rev. 48, 55–69.
- Kloprogge, J.T., Komarneni, S., Amonette, J.E., 1999. Synthesis of smectite clay minerals: a critical review. Clays Clay Miner. 47 (5), 529–554.
- Lee, K.J., 2014. Rigorous simulation model of kerogen pyrolysis for the in-situ upgrading of oil shales.

Lee, K.J., 2019. Characterization of type and maturity of organic matter in source rock by in-situ electrical heating and temperature transient analysis. In: SPE International Conference on Oilfield Chemistry. Society of Petroleum Engineers.

- Lee, K.J., 2020. Characterization of kerogen content and activation energy of decomposition using machine learning technologies in combination with numerical simulations of formation heating. J. Pet. Sci. Eng. 188, 106860.
- Lee, K.J., Finsterle, S., Moridis, G.J., 2018a. Analyzing the impact of reaction models on the production of hydrocarbons from thermally upgraded oil shales. J. Pet. Sci. Eng. 168, 448–464.
- Lee, K.J., Finsterle, S., Moridis, G.J., 2018b. Estimating the reaction parameters of oil shale pyrolysis and oil shale grade using temperature transient analysis and inverse modeling. J. Pet. Sci. Eng. 165, 765–776.
- Lee, K., Moridis, G., Ehlig-Economides, C., 2014. Oil shale in-situ upgrading by steam flowing in vertical hydraulic fractures. In: SPE Unconventional Resources Conference. Society of Petroleum Engineers.
- Lee, K.J., Moridis, G.J., Ehlig-Economides, C.A., 2016a. A comprehensive simulation model of kerogen pyrolysis for the in-situ upgrading of oil shales. SPE J. 21 (05), 1, 612-1, 630.
- Lee, K.J., Moridis, G.J., Ehlig-Economides, C.A., 2016b. In situ upgrading of oil shale by steamfrac in multistage transverse fractured horizontal well system. Energy Sources A 38 (20), 3034–3041.
- Lee, K.J., Moridis, G.J., Ehlig-Economides, C.A., 2017a. Compositional simulation of hydrocarbon recovery from oil shale reservoirs with diverse initial saturations of fluid phases by various thermal processes. Energy Explor. Exploit. 35 (2), 172–193.
- Lee, K.J., Moridis, G.J., Ehlig-Economides, C.A., 2017b. Numerical simulation of diverse thermal in situ upgrading processes for the hydrocarbon production from kerogen in oil shale reservoirs. Energy Explor. Exploit. 35 (3), 315–337.
- Liu, X.M., Li, H., Li, R., Tian, R., Hou, J., 2012. A new model for cation exchange equilibrium considering the electrostatic field of charged particles. J. Soils Sediments 12 (7), 1019–1029.
- Moridis, G.J., 2012. TOUGH+ HYDRATE V1. 2 User's Manual: A Code for the Simulation of System Behavior in Hydrate-Bearing Geologic Media.
- Pawar, G., Meakin, P., Huang, H., 2017. Reactive molecular dynamics simulation of kerogen thermal maturation and cross-linking pathways. Energy Fuels 31 (11), 11601–11614.
- Peiro, L.T., Méndez, G.V., Ayres, R.U., 2013. Lithium: sources, production, uses, and recovery outlook. Jom 65 (8), 986–996.
- Penniston-Dorland, S., Liu, X.-M., Rudnick, R.L., 2017. Lithium isotope geochemistry. Rev. Mineral. Geochem. 82 (1), 165–217.
- Pepper, A.S., Corvi, P.J., 1995. Simple kinetic models of petroleum formation. Part I: oil and gas generation from kerogen. Mar. Pet. Geol. 12 (3), 291–319.
- Pfister, S., et al., 2017. Geochemical and lithium isotope tracking of dissolved solid sources in permian basin carbonate reservoir and overlying aquifer waters at an enhanced oil recovery site, northwest Texas, USA. Appl. Geochem. 87, 122–135.
- Phan, T.T., et al., 2016. Factors controlling li concentration and isotopic composition in formation waters and host rocks of Marcellus Shale, Appalachian Basin. Chem. Geol. 420, 162–179.
- Pistiner, J.S., Henderson, G.M., 2003. Lithium-isotope fractionation during continental weathering processes. Earth Planet. Sci. Lett. 214 (1–2), 327–339.
- Pruess, K., Oldenburg, C.M., Moridis, G., 1999. TOUGH2 User's Guide Version 2.
- Schulz, K.J., DeYoung, J.H., Seal, R.R., Bradley, D.C., 2018. Critical mineral resources of the United States: Economic and environmental geology and prospects for future supply. Geol. Surv..
- Song, L., Carr, T.R., 2020. The pore structural evolution of the Marcellus and Mahantango shales, Appalachian Basin. Mar. Pet. Geol. 114, 104226.
- Starkey, H.C., 1982. The Role of Clays in Fixing Lithium. US Government Printing Office.
- Teichert, Z., Bose, M., Williams, L.B., 2020. Lithium isotope compositions of US coals and source rocks: Potential tracer of hydrocarbons. Chem. Geol. 119694.
- Tissot, B.P., Welte, D.H., 1984. Kerogen: composition and classification. In: Petroleum Formation and Occurrence. Springer, pp. 131–159.
- USGS, 2020. Lithium Data Sheet Mineral Commodity Summaries 2020.
- Vigier, N., Rollion-Bard, C., Levenson, Y., Erez, J., 2015. Lithium isotopes in foraminifera shells as a novel proxy for the ocean dissolved inorganic carbon (DIC). C. R. Geosci. 347 (1), 43–51.
- Vine, J.D., 1975. Lithium in sediments and brines—how, why, and where to search. J. Res. US Geol. Surv. 3 (4), 479–485.
- Williams, L., Clauer, N., Hervig, R., Sylvester, P., 2012. Light stable isotope microanalysis of clays in sedimentary rocks. In: Quantitative Mineralogy and Microanalysis of Sediments and Sedimentary Rocks. Mineralogical Association of Canada Quebec, pp. 55–73.
- Williams, L.B., Hervig, R.L., 2005. Lithium and boron isotopes in illite-smectite: The importance of crystal size. Geochim. Cosmochim. Acta 69 (24), 5705–5716.

K.J. Lee

- Williams, L.B., Środoń, J., Huff, W.D., Clauer, N., Hervig, R.L., 2013. Light element distributions (N, B, Li) in Baltic Basin bentonites record organic sources. Geochim. Cosmochim. Acta 120, 582–599.
- Xiong, Y., et al., 2002. Kinetic simulating experiment on the secondary hydrocarbon generation of kerogen. Sci. China D 45 (1), 13–20.
- Xu, T., Sonnenthal, E., Spycher, N., Pruess, K., 2008. TOUGHREACT User's Guide: A Simulation Program for Non-Isothermal Multiphase Reactive Geochemical Transport in Variably Saturated Geologic Media, V1. 2.1. Lawrence Berkeley National Lab.(LBNL), Berkeley, CA (United States).
- Youtsos, M., Mastorakos, E., Cant, R., 2013. Numerical simulation of thermal and reaction fronts for oil shale upgrading. Chem. Eng. Sci. 94, 200–213.